Modeling of ABS Latex Coagulation Processes

Chang-Bock Chung, Soo-Ho Park, and In-Su Han
Applied Chemical Engineering, Chonnam National University, Kwangju 500-757, Korea

Young-Hyo Seo and Byong-Tae Yang
Styrenic Resins R&D Center, LG Chemical Ltd., Yochon, Chonnam 555-280, Korea

The mathematical models of acrylonitrile–butadiene–styrene (ABS) latex coagulation processes that show the effect of major operation variables on the particle-size distribution of recovered resins were derived to provide a guideline for process improvement to reduce the content of fine particles in the product. Kinetic equations for the coagulation and breakup of particles taking place in a turbulent flow field were incorporated into the population balance models for batch and continuous processes. A dimensional analysis for the process models leads to two dimensionless groups, η_c and η_b, that represent the relative intensity of the coagulation and breakup phenomena. The η_c/η_b ratio is designated as a design variable for controlling the particle-size distribution in the steady-state operation of the coagulation processes. This role is demonstrated by numerical simulation where increasing the ratio shifted the particle-size distribution toward large particles. The estimates of η_c/η_b obtained for a set of batch experiments also confirm that fine particles can be reduced by setting the operation variables to increase the ratio.

Introduction

An acrylonitrile–butadiene–styrene (ABS) latex coagulation process is a postprocessing stage in the manufacturing of ABS resins where the particles are recovered from colloidal latex prepared by emulsion polymerization. Figure 1 shows the atmospheric coagulation process being operated at Yochon plant of LG Chemical Ltd. in Korea. Since the surfaces of the colloidal particles in the latex are negatively charged by adding emulsifiers in the polymerization step, the latex forms a stable colloidal solution by electrostatic repulsion between particles. The particles begin to coagulate into bigger flocs in the coagulator where the repulsive forces are weakened by sulfuric acid added as a coagulant. The coagulated particles overflow into the aging tank and form bigger and more stable flocs at an elevated temperature. The slurry from the aging tank is further processed in the dehydrator and the dryer to the final ABS resin product.

A major concern in the field operation of the process is the excessive content of fine particles in the slurry coming out of the aging tank. The fine particles may be lost in the downstream recovering process, or may cause troubles in processing the recovered resin powder into pellets. Thus, major efforts for process improvement have been directed to the reduction of fine particles in the coagulated slurry. A prerequisite to solving these problems is to comprehend the effect of process operating conditions on the final particle-size distribution.

The purpose of this study is to derive the mathematical models of ABS latex coagulation processes from which one can infer the effect of operation variables on the particle-size distribution of recovered resins. The major operation variables include the slurry content of latex feed, coagulant dosage, agitation speed, residence times, and temperature. The model is expected to provide a guideline for process improvement to reduce the content of fine particles in the product.

To attain the goal we start with kinetic expressions for coagulation and breakup phenomena taking place in a turbulent flow field. The kinetic equations are then incorporated into the population balance models for batch and continuous processes. The process models, when converted into a dimensionless form, have two sorts of dimensionless groups, η_c and η_b, which characterize the relative intensity of the coagulation and breakup as affected by the operation variables.

Correspondence concerning this article should be addressed to C.-B. Chung.

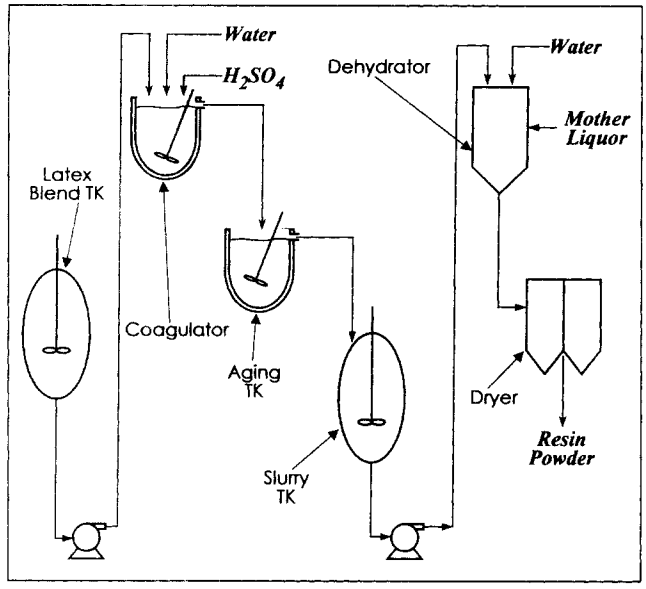

Figure 1. Atmospheric ABS latex coagulation process.

Hence the η_c/η_b ratio acts as a design variable for controlling the particle-size distribution in the steady-state operation of the process. This role is demonstrated by numerical simulation and batch experiments.

Process Modeling

Kinetic equations

The surfaces of colloidal particles in ABS latex are charged with negative ions, and thus keep stable distribution due to electrostatic repulsion between the particles. The addition of coagulants decreases the repulsive forces and brings about the coagulation of particles. The coagulation takes place through the following two steps: (1) a transport step in which particles are brought into the close proximity of each other; and (2) a coalescence step in which the close particles are bound together by short-range interfacial forces. Transport mechanisms are usually provided by Brownian motions or velocity gradients formed by fluid shear. Coalescence results from complicated interaction among hydrodynamic forces, electrostatic forces, and van der Waals forces, among others.

The time evolution of the size distribution in a coagulating population of particles is customarily described by (Valioulis, 1986; Gillespie, 1972)

$$\frac{dn(v)}{dt} = \frac{1}{2}\int_0^v \beta(u, v-u)n(u)n(v-u)\,du - n(v)\int_0^\infty \beta(v,u)n(u)\,du, \quad (1)$$

where $n(v)$ denotes a distribution function for the number concentration of particles of volume v (i.e., $n(v)dv$ is the number concentration of particles of volume between v and $v+dv$), and $\beta(v,u)$ is the collision frequency function for particles of size v and u. The first term on the righthand side of Eq. 1 represents the formation of particles of size v by collisions of smaller particles, and the second term denotes the loss of particles of size v by collision with particles of any other size.

The coagulator and the aging tank of the ABS latex coagulation process shown in Figure 1 are operated under intense agitation to assure thorough mixing and high collision frequency between particles. The collision frequency function $\beta(v,u)$ for such turbulent shear-induced coagulation is known to take the following form (Saffman and Turner, 1956):

$$\beta(v,u) = 0.31G(v^{1/3}+u^{1/3})^3\alpha. \quad (2)$$

In the preceding equation, G denotes the spatially averaged velocity gradient (Camp and Stein, 1943) and, for an agitated vessel, can be correlated by (Ives, 1981)

$$G = \sqrt{\frac{P}{V\mu}}, \quad (3)$$

where P is the agitation power, V the fluid volume, and μ the fluid viscosity. α denotes the collision efficiency that accounts for the fact that all the collisions do not necessarily result in the coalescence of particles.

It is well known that the coagulation phenomena are accompanied by the so-called floc breakup phenomenon where a big, coagulated particle breaks into smaller particles in the presence of hydrodynamic stresses arising from turbulent shear. Floc breakup takes the form of (1) *splitting* into a few smaller particles, and (2) *erosion* of fine particles from the surface of a big particle (Quigley and Spielman, 1977).

The major elements in the modeling of floc breakup are the breakup rate and the particle-size distribution of daughter particles. A kinetic model that incorporates the modeling elements can be postulated as follows (Spicer and Pratsinis, 1996):

$$\frac{dn(v)}{dt} = -S(v)n(v) + \int_v^\infty \Gamma(v,u)S(u)n(u)\,du, \quad (4)$$

where $S(v)$ is the breakup rate of floc of size v, and $\Gamma(v,u)$ is the breakage distribution function defining the volume fraction of the fragments of size v coming from flocs of size u. Hence the first righthand side term represents the loss of particles of size v by breakup, and the second term represents the formation of particles of size v by the breakup of larger particles.

The inherent intricacies associated with turbulence phenomena make deriving theoretical expressions for $S(v)$ and $\Gamma(v,u)$ a formidable task. Hence any model for these terms will necessarily contain unknown model parameters that should be estimated on the basis of experimental data. In this respect the model proposed by Spielman and coworkers (Pandya and Spielman, 1982; Lu and Spielman, 1985) seems

to represent the maximum rigor one can think of for the modeling of floc breakup: their model consists of complicated expressions of $S(v)$ and $\Gamma(v,u)$ for each of the splitting and erosion mechanisms of floc breakup, and contains a total of 11 adjustable parameters. Obtaining the estimates of so many parameters does not look feasible unless a very large amount of experimental data is available.

In this study we adopted a rather simple approach that was proposed in the literature (Spicer and Pratsinis, 1996; Chen et al., 1990). Specifically, we neglect the erosion mechanism of floc breakup on the basis of the physical intuition that splitting dominates breakup in turbulent flows. We further assume binary breakage where every breakup results in the formation of two daughter particles of equal size. Accordingly $S(v)$ and $\Gamma(v,u)$ are assumed to take the following forms in our model:

$$S(v) = AG^{y}v^{a} \tag{5}$$

$$\Gamma(v,u) = 2\delta(v - 0.5u), \tag{6}$$

where A is a proportionality constant; y is a parameter that measures the fragility of flocs facing turbulent shear; a is a parameter that reflects the relative weakness of large-sized flocs in comparison with smaller flocs; and δ denotes the Dirac delta function. These parameters pertain to the characteristics of a particulate system being investigated, and thus should be determined on the basis of experimental data.

Combining Eqs. 1 and 4, we obtain a kinetic model for the coagulation and breakup of particles taking place simultaneously in a flocculating suspension:

$$\frac{dn(v)}{dt} = \frac{1}{2}\int_0^v \beta(u, v-u)n(u)n(v-u)\,du - n(v)\int_0^\infty \beta(v,u)n(u)\,du - S(v)n(v) + \int_v^\infty \Gamma(v,u)S(u)n(u)\,du. \tag{7}$$

Equation 7 is to be incorporated in the population balance for batch and continuous processes to obtain the respective process models.

Discretization of kinetic equations

In order to obtain a numerical solution of the kinetic model, it is necessary to convert the equation into a discrete form of amenable size. The first step of the conversion is to divide the continuous particle-size spectrum into a finite number of *size classes* or *sections*. Then, the conservation law is applied to each section to get a set of sectional balance equations. The sectioning scheme determines the type of the sectional balance equations and the level of difficulty in constructing the corresponding numerical algorithms.

We adopted the sectional balance approach, which Gelbard et al. (1980) proposed, to solve the coagulation kinetics as given in Eq. 1, and extended it to cover our breakup kinetics included in Eq. 7 as well. The approach is quite general in the following three senses: (1) there is no limitation in locating the section boundaries dividing the whole particle spectrum; (2) one can use an arbitrary measure of particle size such as volume, diameter, or others; (3) the balance may be set up with respect to an arbitrary particle property such as volume, surface area, or numbers.

The detailed procedure of deriving the general sectional balance equations is well documented by Gelbard et al. (1980); here we summarize the key steps and refer interested readers to the cited paper for more details.

1. Divide the whole range of particle volumes into m sections.

2. Introduce a distribution function $q(v)$ for a general property:

$$q(v) = cv^{r}n(v), \tag{8}$$

where $q(v)$ is simply equal to $n(v)$ when $c = 1$ and $r = 0$; it also represents the surface distribution if $c = \pi^{1/3}6^{2/3}$ and $r = 2/3$ and the volume distribution if $c = 1$ and $r = 1$.

3. Define an integral quantity Q_l for each section to be conserved

$$Q_l = \int_{v_{l-1}}^{v_l} q(v)\,dv, \qquad l = 1,2,\ldots,m. \tag{9}$$

4. Derive a general conservation equation for Q_l by determining the change in the property $q(v)$ due to coagulation and breakup.

5. Change the measure of particle size from the volume v to an arbitrary variable x by defining a transformation of the form

$$x = f(v). \tag{10}$$

6. Assume that q has a uniform distribution with respect to x within each section, that is,

$$q(v) = \bar{q}_l f'(v), \tag{11}$$

where $\bar{q}_l$ is a constant. Then the following relationship can be derived from Eqs. 8–11:

$$n(v) = \frac{Q_l f'(v)}{cv^{r}(x_l - x_{l-1})}. \tag{12}$$

7. Substitute Eq. 12 in the conservation equation obtained in step 4.

Note that the assumption made in step 6 corresponds to the lowest-order discretization scheme. A plot of q vs. x results in a series of step functions. It can be compared to a simple finite difference scheme for solving boundary-value problems. Of course, one may also choose a higher-order distribution function (e.g., linear splines) to obtain a more accurate solution, but at the cost of increasing effort for mathematical processing and computation. Here the major objec-

tive of our sectional representation is to obtain a reasonably accurate solution with a minimum amount of effort.

The sectional balance equations derived by the preceding procedure are summarized as follows:

$$\frac{dQ_1}{dt} = -\frac{1}{2}{}^3\bar{\beta}_{1,1}Q_1^2 - Q_1\sum_{i=2}^{m}{}^4\bar{\beta}_{i,1}Q_i - {}^1\bar{S}_1Q_1 + \sum_{i=2}^{m}{}^2\bar{S}_{i,1}Q_i$$

$$\frac{dQ_l}{dt} = \frac{1}{2}\sum_{i=1}^{l-1}\sum_{j=1}^{l-1}{}^1\bar{\beta}_{i,j,l}Q_iQ_j - Q_l\sum_{i=1}^{l-1}{}^2\bar{\beta}_{i,l}Q_i - \frac{1}{2}{}^3\bar{\beta}_{l,l}Q_l^2 - Q_l\sum_{i=l+1}^{m}{}^4\bar{\beta}_{i,l}Q_i - {}^1\bar{S}_lQ_l + \sum_{j=l+1}^{m}{}^2\bar{S}_{i,l}Q_i, \quad l = 2, \ldots, m-1$$

$$\frac{dQ_m}{dt} = \frac{1}{2}\sum_{i=1}^{m-1}\sum_{j=1}^{m-1}{}^1\bar{\beta}_{i,j,m}Q_iQ_j - Q_m\sum_{i=1}^{m-1}{}^2\bar{\beta}_{i,m}Q_i - \frac{1}{2}{}^3\bar{\beta}_{m,m}Q_m^2 \quad (13)$$

Equation 13 contains four sorts of coagulation coefficients (${}^1\bar{\beta}_{i,j,l}$, ${}^2\bar{\beta}_{i,l}$, ${}^3\bar{\beta}_{l,l}$, ${}^4\bar{\beta}_{i,l}$) and two sorts of breakup coefficients (${}^1\bar{S}_l$, ${}^2\bar{S}_{i,l}$) that should be evaluated by the integrals listed in Table 1. It should be noted that the integral expressions in Table 1 were obtained under the so-called *geometric sectionalization*, where a geometric constraint is imposed on the section boundaries (i.e., $\nu_i \geq 2\nu_{i-1}$, $i = 1, 2, \ldots, m$). Although the section boundaries can be arbitrarily set up, the geometric sectioning is considered to be a practical and efficient scheme for very large size ranges encountered in most coagulation systems.

Batch process model

A model for a specific coagulation process is generally obtained by setting up mass balance around the process unit where the accumulation term is equated with the input/output and generation terms combined. Since a batch process does not have any input or output flow, the process model can be equated with the kinetic equations given in Eq. 13. Here the batch process model is intended to represent our lab-scale experiments to be described later.

Table 1. Coagulation/Breakup Coefficients with Geometric Constraint

Symbol	Remarks	Coefficient
${}^1\bar{\beta}_{i,j,l}$	$i < l-1$ $j < l-1$	0
${}^1\bar{\beta}_{i,l-1,l}$	$2 \leq l \leq m$ $i < l-1$	$\int_{x_{i-1}}^{x_i}\int_{f(\nu_{l-1}-\nu)}^{x_{l-1}} \frac{(u+\nu)^r\beta(u,\nu)}{cu^r\nu^r(x_i-x_{i-1})(x_{l-1}-x_{l-2})}dydx$
	$2 \leq l \leq m$ $i = l-1$	$\int_{x_{i-1}}^{f(\nu_i-\nu_{i-1})}\int_{f(\nu_{l-1}-\nu)}^{x_{l-1}} \frac{(u+\nu)^r\beta(u,\nu)}{cu^r\nu^r(x_i-x_{i-1})(x_{l-1}-x_{l-2})}dydx + \int_{f(\nu_i-\nu_{i-1})}^{x_i}\int_{x_{l-2}}^{x_{l-1}} \frac{(u+\nu)^r\beta(u,\nu)}{cu^r\nu^r(x_i-x_{i-1})(x_{l-1}-x_{l-2})}dydx$
${}^2\bar{\beta}_{i,l}$	$2 \leq l \leq m$ $i < l$	$\int_{x_{i-1}}^{x_i}\int_{f(\nu_l-\nu)}^{x_l} \frac{u^r\beta(u,\nu)}{cu^r\nu^r(x_i-x_{i-1})(x_l-x_{l-1})}dydx - \int_{x_{i-1}}^{x_i}\int_{x_{l-1}}^{f(\nu_l-\nu)} \frac{[(u+\nu)^r-u^r]\beta(u,\nu)}{cu^r\nu^r(x_i-x_{i-1})(x_l-x_{l-1})}dydx$
${}^3\bar{\beta}_{l,l}$	$1 \leq l \leq m$	$\int_{x_{l-1}}^{f(\nu_l-\nu_{l-1})}\int_{f(\nu_l-\nu)}^{x_l} \frac{(u^r+\nu^r)\beta(u,\nu)}{cu^r\nu^r(x_l-x_{l-1})^2}dydx + \int_{f(\nu_l-\nu_{l-1})}^{x_l}\int_{x_{l-1}}^{x_l} \frac{(u^r+\nu^r)\beta(u,\nu)}{cu^r\nu^r(x_l-x_{l-1})^2}dydx + \int_{x_{l-1}}^{f(\nu_l-\nu_{l-1})}\int_{x_{l-1}}^{f(\nu_l-\nu)} \frac{[u^r+\nu^r-(u+\nu)^r]\beta(u,\nu)}{cu^r\nu^r(x_l-x_{l-1})^2}dydx$
${}^4\bar{\beta}_{i,l}$	$1 \leq l < m$ $l < i$	$\int_{x_{i-1}}^{x_i}\int_{x_{l-1}}^{x_l} \frac{u^r\beta(u,\nu)}{cu^r\nu^r(x_i-x_{i-1})(x_l-x_{l-1})}dydx$
${}^1\bar{S}_l$	$1 \leq l \leq m$	$\int_{x_{l-1}}^{f(2\nu_{l-1})} \frac{S(\nu)}{x_l-x_{l-1}}dx + \int_{f(2\nu_{l-1})}^{x_l} \frac{(1-2(0.5)^r)S(\nu)}{x_l-x_{l-1}}dx$
${}^2\bar{S}_{i,l}$	$1 \leq l < m$ $i = l+1$	$\int_{x_{i-1}}^{f(2\nu_l)} \frac{2(0.5)^rS(\nu)}{x_i-x_{i-1}}dx$
	$1 \leq l < m$ $l+1 \leq i$	0

Equation 13 was converted into a dimensionless form before attempting to construct a numerical algorithm. First we define the dimensionless variables as follows:

$$\begin{cases} \tilde{Q}_l = Q_l/Q_0 & \text{where} \quad Q_0 = c\nu_0^r n_0 \\ \tilde{t} = t/t_0 & \text{where} \quad t_0 = \text{batch duration} \\ \bar{\tilde{\beta}} = \bar{\beta}/\bar{\beta}_0 & \text{where} \quad \bar{\beta}_0 = \alpha G \nu_0 / c\nu_0^r \\ \bar{\tilde{S}} = \bar{S}/\bar{S}_0 & \text{where} \quad \bar{S}_0 = AG^y \nu_0^a, \end{cases} \tag{14}$$

where ν_0 denotes the volume of the primary particle and n_0 the total number concentration of the primary particles in the latex. Accordingly the product of ν_0 and n_0 is equal to the volume fraction of the solids in the latex, which we call the slurry content, ϕ. Substituting Eq. 14 into Eq. 13 and rearranging, we get

$$\frac{d\tilde{Q}_1}{d\tilde{t}} = \eta_c \times \left[-\frac{1}{2}{}^3\bar{\tilde{\beta}}_{1,1}\tilde{Q}_1^2 - \tilde{Q}_1 \sum_{i=2}^{m} {}^4\bar{\tilde{\beta}}_{i,1}\tilde{Q}_i \right] + \eta_b \times \left[-{}^1\bar{\tilde{S}}_1\tilde{Q}_1 + \sum_{i=2}^{m} {}^2\bar{\tilde{S}}_{i,1}\tilde{Q}_i \right]$$

$$\frac{d\tilde{Q}_l}{d\tilde{t}} = \eta_c \times \left[\frac{1}{2}\sum_{i=1}^{l-1}\sum_{j=1}^{l-1} {}^1\bar{\tilde{\beta}}_{i,j,l}\tilde{Q}_i\tilde{Q}_j - \tilde{Q}_l \sum_{i=1}^{l-1} {}^2\bar{\tilde{\beta}}_{i,l}\tilde{Q}_i - \frac{1}{2}{}^3\bar{\tilde{\beta}}_{l,l}\tilde{Q}_l^2 - \tilde{Q}_l \sum_{i=l+1}^{m} {}^4\bar{\tilde{\beta}}_{i,l}\tilde{Q}_i \right] + \eta_b \times \left[-{}^1\bar{\tilde{S}}_l\tilde{Q}_l + \sum_{i=l+1}^{m} {}^2\bar{\tilde{S}}_{i,l}\tilde{Q}_i \right], \quad l = 2, \ldots, m-1$$

$$\frac{d\tilde{Q}_m}{d\tilde{t}} = \eta_c \times \left[\frac{1}{2}\sum_{i=1}^{m-1}\sum_{j=1}^{m-1} {}^1\bar{\tilde{\beta}}_{i,j,m}\tilde{Q}_i\tilde{Q}_j - \tilde{Q}_m \sum_{i=1}^{m-1} {}^2\bar{\tilde{\beta}}_{i,m}\tilde{Q}_i - \frac{1}{2}{}^3\bar{\tilde{\beta}}_{m,m}\tilde{Q}_m^2 \right] + \eta_b \times \left[-{}^1\bar{\tilde{S}}_m\tilde{Q}_m \right] \tag{15}$$

$$I.C.: \quad \tilde{Q}_l(0) = \tilde{Q}_{l,0}, \qquad l = 1, \ldots, m \tag{16}$$

where

$$\eta_c = Q_0 t_0 \bar{\beta}_0 = \alpha\phi G t_0$$
$$\eta_b = \bar{S}_0 t_0 = AG^y \nu_0^a t_0. \tag{17}$$

In Eq. 16, $\tilde{Q}_{l,0}$ denotes the particle-size distribution of the latex before coagulation.

Equation 15 can be recast

$$\frac{d\tilde{Q}_l}{d\tilde{t}} = \eta_c \cdot f_c(\tilde{Q}) + \eta_b \cdot f_b(\tilde{Q}), \tag{18}$$

where $f_c(\tilde{Q})$ and $f_b(\tilde{Q})$ denote the respective dynamics of coagulation and breakup represented by the terms enclosed in square brackets in Eq. 15, and η_c and η_b represent the dimensionless group associated with each phenomenon. As shown in Eq. 17, η_c consists of the collision efficiency α, the slurry content ϕ in the latex, the spatially averaged velocity gradient G, and the batch duration t_0. This means that the product of these factors will collectively determine the rate of coagulation. Similarly, η_b given as the product of the breakup rate $AG^y\nu_0^a$ and t_0 determines the rate of floc breakup. Hence it can be stated that the ratio of the dimensionless groups η_c/η_b represents the relative intensity of coagulation and breakup phenomena taking place in the system. Recalling that the steady-state solution of Eq. 15 is obtained by equating the righthand side terms to zero, it will be readily understood that the η_c/η_b ratio will be a deciding factor for the steady-state particle-size distribution. The magnitude of either η_c or η_b will determine the speed at which the time-evolving particle-size distribution reaches the ultimate state.

It is noteworthy that Spicer et al. (1996) defined a similar dimensionless group, called a *coagulation–fragmentation* (CF) *group*, that characterizes the relative significance of coagulation vs. fragmentation in a flocculating suspension. The group CF, which was derived in a different fashion from ours, corresponds to 2.48 times the reciprocal of the η_c/η_b ratio. Spicer et al. then investigated the geometric standard deviation for the number- and volume-based particle-size distributions and the time lag for attainment of steady-state as a function of the group.

Continuous process model

The core parts of the ABS latex coagulation process shown in Figure 1 are the coagulator and the aging tank. The two vessels are operated in continuous mode and can be described by "two CSTRs in-series" as shown in Figure 2. The model of this continuous process was obtained by setting up population balances for each tank and then by converting them into a dimensionless form:

$$\begin{cases} \dfrac{d\tilde{Q}_l^{(1)}}{d\tilde{t}} = \tilde{Q}_l^{\text{in}} - \tilde{Q}_l^{(1)} + \eta_{c_1} \cdot f_c(\tilde{Q}^{(1)}) + \eta_{b_1} \cdot f_b(\tilde{Q}^{(1)}) \\ \dfrac{d\tilde{Q}_l^{(2)}}{d\tilde{t}} = \tilde{Q}_l^{(1)} - \tilde{Q}_l^{(2)} + \eta_{c_2} \cdot f_c(\tilde{Q}^{(2)}) + \eta_{b_2} \cdot f_b(\tilde{Q}^{(2)}) \end{cases} \tag{19}$$

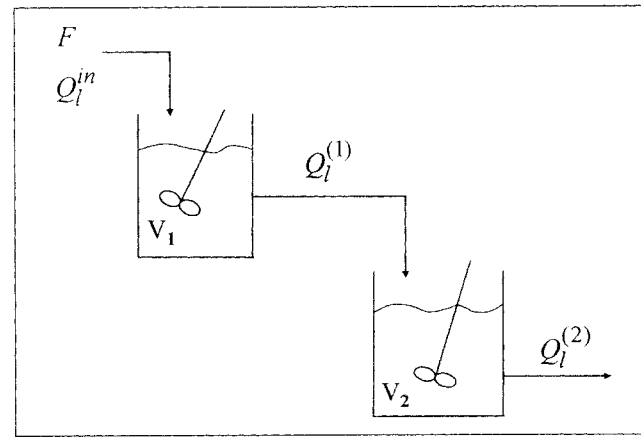

Figure 2. Two CSTRs in-series model for the coagulator and the aging tank.

$$I.C.: \quad \tilde{Q}_l^{(1)}(0) = \tilde{Q}_{l,0}^{(1)}$$
$$\tilde{Q}_l^{(2)}(0) = \tilde{Q}_{l,0}^{(2)} \tag{20}$$

where

$$\eta_{c_1} = \alpha\phi G_1\tau_1, \qquad \eta_{c_2} = \alpha\phi G_2\tau_2$$
$$\eta_{b_1} = AG_1^y v_0^a\tau_1, \qquad \eta_{b_2} = AG_2^y v_0^a\tau_2 \tag{21}$$

where

$$\tau_1 = V_1/F$$
$$\tau_2 = V_2/F. \tag{22}$$

In Eq. 22, F denotes the volumetric flow rate of the latex feed, and V_1, V_2 and τ_1, τ_2 denote the volumes and residence times of the first and second tank, respectively.

The dynamics of each tank consists of the input/output terms and the kinetic terms. The kinetic terms have the same dynamics as in the batch model except that the residence times τ_1 and τ_2 replace the batch duration t_0. The model has four dimensionless groups, two for each tank. Under the circumstances, where the input/output terms are negligible in magnitude compared to the kinetic terms, the overall dynamics will be governed by the latter. In this case, which holds true especially for high slurry content and large residence times, the steady-state particle-size distribution is again determined by the ratios of dimensionless groups η_{c_1}/η_{b_1} and/or η_{c_2}/η_{b_2}. This situation is demonstrated by the numerical simulation presented in the next section.

The present process model, summarized by Eqs. 19–22, does not take into account all the variables considered in the field operation. Among the operation variables, the slurry content (ϕ) and the particle-size distribution (Q_l^{in}) of the inflowing latex, the turbulent shear rates (G_1, G_2), and the residence times (τ_1, τ_2) are treated as direct input data for the model. On the other hand, the coagulant dosage is indirectly reflected through its contribution to enhancing the collision efficiency α. Due to the very complicated interaction mechanism between colliding particles, however, it has not been feasible to establish a quantitative relationship between α and the coagulant dosage or other variables.

Finally, the temperature of each tank is not taken into account at all in the current model. The coagulator is normally operated between 80 and 85°C in the field, while the aging tank is operated at an elevated temperature around 95°C. This high temperature, which is about 10°C below the glass transition temperature of the styrene–acrylonitrile (SAN) resin phase of the ABS particles, is believed to promote the entanglement of the SAN chains protruding from the component particles in the coagulated floc. The chain entanglement is regarded as a core *aging* mechanism that renders the floc stable against fragmentation. The effect of temperature on coagulation and breakup kinetics, which has not been investigated much in the literature, was excluded from the scope of this study.

Numerical Simulation

In this section we present the results of numerical simulation for the batch and continuous processes. The purpose of the simulation is to investigate the effect of operation variables and model parameters on the particle-size distribution of recovered resins under the base conditions approximating the field operation.

In our simulation the whole particle-size spectrum, with diameters ranging from 0.1 μm to 3 mm, was divided into 46 intervals, with the volume boundaries located in a geometric sequence of ratio 2. All the particles were assumed to keep a spherical shape. The particle diameter was selected as the size variable (x), and the volume was chosen as the property to be conserved ($c = 1$, $r = 1$).

The coagulation and breakup coefficients given by the integrals in Table 1 were evaluated using the two-dimensional Gauss–Legendre quadrature algorithm (Press et al., 1986) with 100 evaluation points along each dimension. Then the initial-value problems defined by Eqs. 15–17 or Eqs. 19–22 were solved using an LSODE routine (Hindmarsh, 1980). About eight minutes of CPU time were required to carry out one run of simulation on a Pentium 166 machine with most of the time consumed in the evaluation of the coefficients. Once the coefficients are evaluated off-line, however, they can be stored and used again in the subsequent runs.

The base operating conditions used in our numerical simulation were adopted from the field operation. The ABS latex coming from the upstream emulsion polymerization process has its own size distribution ranging from 0.1 μm to 3.2 μm. The latex fed to the coagulator has slurry content of 23%, which corresponds to the very high total concentration, $n_0 = 4.39\times10^{20}$ m^{-3}, of primary particles. The spatially averaged velocity gradient G was found to be approximately 40 s^{-1}.

For the model parameters the following values were tentatively assumed: $\alpha = 1$, $A = 200$, $y = 1.5$, $a = 1/3$. $\alpha = 1$ means that all the collisions between particles lead to coagulation, that is, the maximum coagulation rate is assumed. The other parameters are associated with floc breakup kinetics. The assumed value for a is consistent with the theoretical expectation that breakage is proportional to the particle diameter (Spicer and Pratsinis, 1996; Boadway, 1978). The y value was also adopted from Spicer and Pratsinis (1996), who estimated $y = 1.6\pm0.18$ at $G = 25$–150 s^{-1} for flocculation of monodisperse polystyrene latex by regressing the experimental data of Oles (1992). Then the value of A was found by trial-and-error runs that reasonably matched the steady-state particle-size distributions obtained in field operation of the process.

Figure 3 shows the transient particle-size distributions in a batch process evolving from the initial polydisperse distribution of the latex to the final steady state. In order to show clearly the rapid dynamics observed in an earlier stage, we intentionally represented the distributions in terms of volume percent vs. section number. The distributions were found to shift to the right with increasing time and to reach the steady state in about 10 s.

Numerous simulation runs have been carried out to investigate the effects of the operation variables and the model parameters. But, recalling the earlier statement that these effects manifest themselves through the contribution to each of the dimensionless groups η_c and η_b, we feel it enough here to present only the results showing the effects of η_c and η_b. The magnitude of either η_c or η_b characterizes how fast the system evolves while the η_c/η_b ratio determines the shape of the steady-state particle-size distribution. Figure 4 shows the

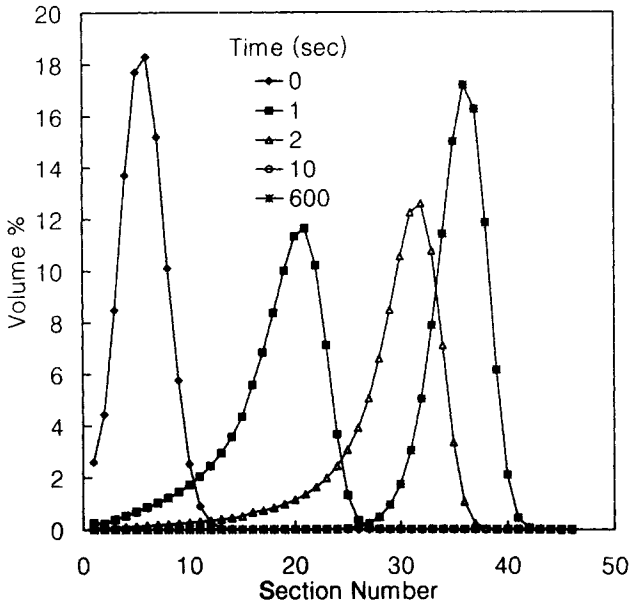

Figure 3. Evolution of the particle-size distribution in a batch process.

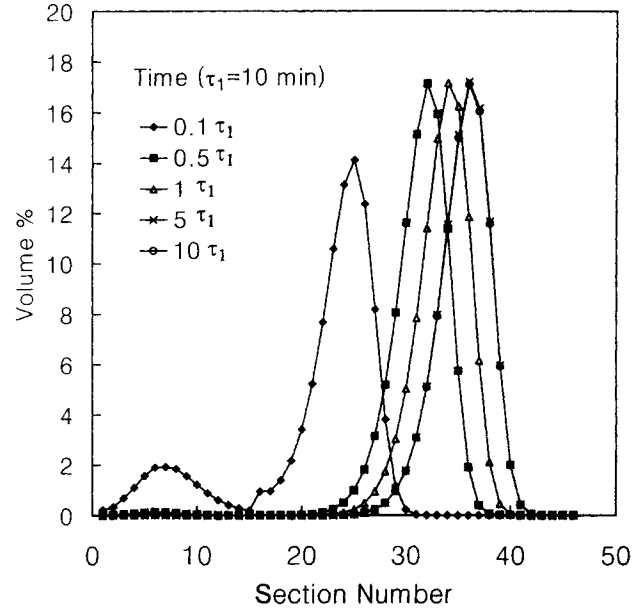

Figure 5. Evolution of the particle-size distribution in the first tank of a continuous process.

steady-state distributions corresponding to three different levels of the ratio. As the ratio increases, coagulation phenomena have an increasing edge over breakup, thus shifting the distribution toward larger particles. It should be noted that all the curves have a similar shape and only differ in the locations of the peaks. This is consistent with the findings of Spicer et al. (1996), who reported that the steady-state geometric standard deviations of volume-based distributions exhibited little change over a wide range of CF groups.

In the remainder of this section we present the simulation results for the continuous process shown in Figure 2. The residence time of each tank was set to 10 and 50 min, respectively, to simulate the field operation. The other conditions were assumed to be the same as in the batch process simulation.

Figures 5 and 6 describe the transient situations that would be observed in each tank during a startup period. They show the time-evolving particle-size distributions in each tank initially filled with water. The distribution in each tank was found to almost reach the steady state after five times the respective residence time.

A close comparison between Figures 5 and 6 reveals that the two tanks had almost identical steady-state particle-size distributions. In other words, the inlet stream to the second tank showed the same distribution as the outlet stream at

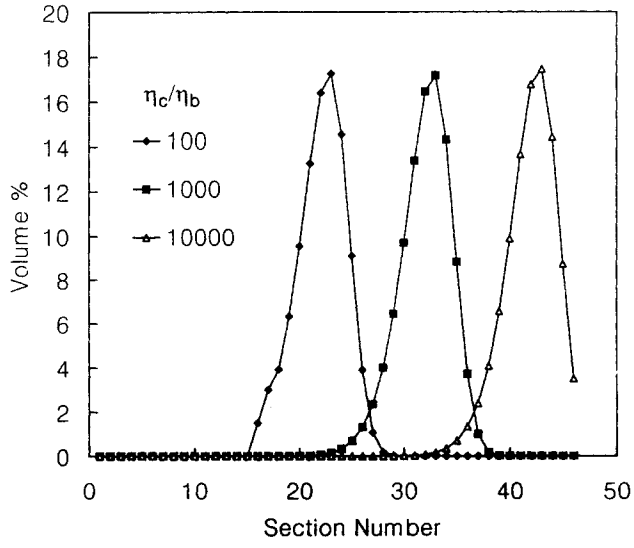

Figure 4. Effect of the η_c/η_b ratio on the steady-state particle-size distribution.

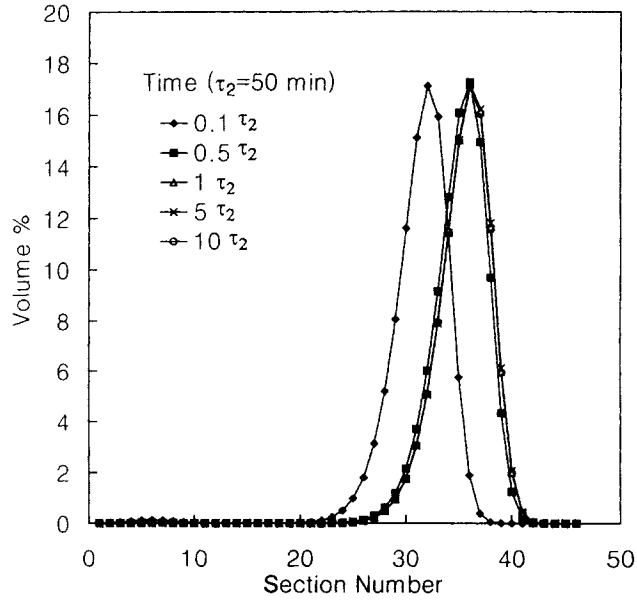

Figure 6. Evolution of the particle-size distribution in the second tank of a continuous process.

steady state under the current operating conditions. This conforms to a field observation that most changes in particle-size distribution from the latex state to the recovered resin are found to take place in the coagulator; the aging tank provides an environment within which loosely bound particles are tied together at an elevated temperature to form a stable floc.

To investigate the reason for the identical distribution discussed before, let us examine the dynamics given in Eq. 19 with a focus on the first tank. As mentioned in the modeling section, the righthand side of the equations comprises two components, the input/output terms $(\tilde{Q}_i^{\text{in}} - \tilde{Q}_i^{(1)})$ and the kinetic terms $[\eta_{c_1} f_c(\tilde{Q}^{(1)}) + \eta_{b_1} f_b(\tilde{Q}^{(1)})]$. Under the current simulation conditions the magnitude of the input/output terms for each section was found to be more than a hundred times smaller than that of the kinetic terms. Such a big difference means that the dynamics of the vessel is governed by the kinetics, and thus implies that the steady-state distribution in a continuously operated tank will approximate the distribution that would be obtained in a batch operation of the same unit. This point can be confirmed by noticing the indistinguishable steady-state distributions between the batch and continuous modes shown in Figures 3 and 5.

In this respect it is worth investigating the effect of residence time on steady-state distribution. Figure 7 shows the steady-state distributions of the first tank calculated using different values of τ_1. It can be seen that the distributions obtained at small τ_1 are influenced not only by the kinetics but also by the inflow of latex. The latter effect almost vanishes as τ_1 goes up to 3 min and above. Thus the steady-state distribution is determined by the kinetic terms for a sufficiently large residence time. Since τ_1 and τ_2 in Eq. 21 are canceled out between like ones when taking the η_{c_1}/η_{b_1} and η_{c_2}/η_{b_2} ratios, respectively, it follows that the steady-state distribution will not be affected by the magnitude of τ_1 or τ_2 once either one reaches a sufficient level.

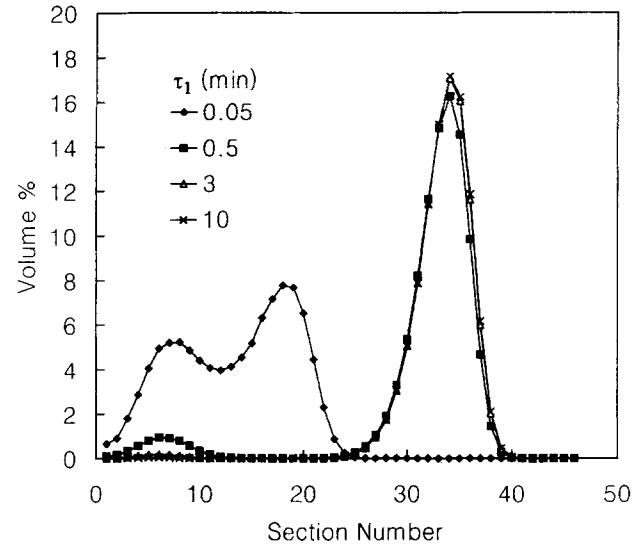

Figure 7. Effect of the residence time on the steady-state particle-size distribution in the first tank.

Experimental Verification

A series of batch coagulation experiments were carried out to check the validity of the model predictions concerning the effects of operation variables on particle-size distribution. Table 2 lists the values of three operation variables manipulated in these experiments. In each run ABS latex solution was poured into an agitated 2-L vessel containing a preset amount of sulfuric acid solution. The temperature was maintained at around 90°C for 30 min to allow sufficient aging of the coagulated flocs, and then the slurry was dehydrated and dried to recover the resin powder. The coagulation was observed to proceed very fast due to the high slurry content of the latex, but unfortunately we did not have any device to measure the time-evolving particle-size distributions of the slurry. Only the steady-state distribution of the recovered resin was measured using a stack of 18 meshes with the scales ranging from 7 (2.83 mm in diameter) to 325 (0.044 mm).

Our kinetic model contains four unknown model parameters (α, A, y, a) that have to be estimated on the basis of experimental data. α is associated with the coagulation kinetics, and the other three with the breakup kinetics. It is evident that the steady-state particle-size distributions measured in our experiments do not provide enough information to identify all these parameters. Even a simplified task of estimating η_c and η_b instead of the original model parameters would face inherent nonuniqueness problems without sufficient dynamic data; at most, the η_c/η_b ratio may be determined uniquely when only steady-state size distribution is available.

Estimating only the η_c/η_b ratio, which best explains the outcome of each experiment, may not sound so meaningful in the usual sense of model parameter estimation, because the purpose of parameter estimation is to enable one to predict the outcome under different conditions. Nonetheless, such an estimation job will provide a basis for evaluating the role of the η_c/η_b ratio as a design variable in controlling the steady-state particle-size distribution.

The least-squares method was used to estimate the η_c/η_b ratio that would best fit the observed particle-size distribution for each experiment. Specifically, the value of η_c/η_b that minimizes the following objective function was found

$$J(\eta_c/\eta_b) = \sum_{j=1}^{M} \left[\frac{\text{vol}_j^{\text{obs}}}{\Delta d_j} - \frac{\text{vol}_j^{\text{calc}}\,(\eta_c/\eta_b)}{\Delta d_j} \right]^2, \qquad (23)$$

where $\text{vol}_j^{\text{obs}}$ and $\text{vol}_j^{\text{calc}}$ denote, respectively, the measured and calculated volume fraction of the particles on the jth mesh, and Δd_j denotes the difference in diameter between

Table 2. Operation Variables and Estimates of η_c/η_b for Batch Experiments

Run No.	Oper. Var. ϕ	rpm	HS	Meas. Vol. % Below 200 Mesh	Above 20 Mesh	Minimiz. Status $J_{\min}$	Est. η_c/η_b
1	0.15	300	1.5	4.58	7.54	9.2×10^{-6}	1,467
2	0.15	220	1.5	4.15	22.78	5.8×10^{-6}	2,810
3	0.15	150	1.5	0.63	46.53	2.2×10^{-6}	4,478
4	0.20	150	1.5	0.17	55.68	9.6×10^{-6}	5,342
5	0.15	220	2.3	1.2	43.9	1.2×10^{-6}	4,743

the jth and $(j+1)$th meshes. The differential particle-size distribution was used in the objective function J in order to make the estimate better match the observed distribution on the fine particle side rather than on the coarse side. This scheme is expected to better serve the objective of our study, which is to predict the contents of fine particles in the product.

Table 2 lists the estimated values of η_c/η_b and the corresponding objective functions for the batch experiments. Figure 8 compares the particle-size distribution calculated using the estimated value of η_c/η_b with the measured distribution for Run 1. A good match was obtained between the two on the fine particle side, but there was a significant deviation on the other side. A similar trend was also observed for Runs 2–5. The failure of the model output to match the details of the measured distribution over the whole size range can be attributed to the modeling errors caused by the simplifying assumptions introduced in our study. The major errors seem to be associated with our simplified breakup kinetics. Specifically, we neglected (1) the erosion mechanism that might lead to a bimodal distribution with large and small fragments, (2) the possibility of a floc splitting into more than two particles, and (3) nonlinear breakup due to collisions between agglomerates. Other possible sources of error would be the assumptions of constant collision efficiency and perfect mixing in the agitated tanks.

The effects of operation variables on the particle-size distribution are reflected in the measured volume percents of very fine particles below 200 mesh (0.074 mm) and coarse particles above 20 mesh (0.841 mm). Comparison among Runs 1–3 shows that raising the agitation speed results in an increase of fine particles along with a decrease of coarse ones. The comparison between Runs 3 and 4 demonstrates that the increase of the slurry content in the latex led to the formation of more coarse particles. A similar effect was found for the coagulant dosage when comparing Runs 2 and 5. Notice that all these effects of the operation variables conform to our model prediction that fine particles can be reduced by

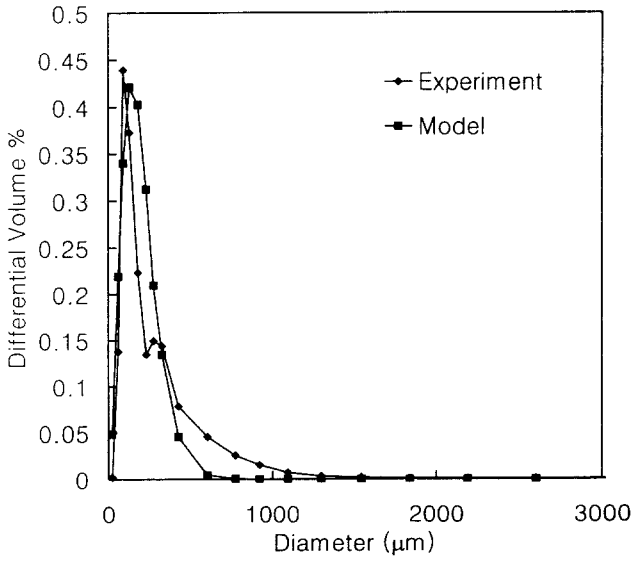

Figure 8. Model predictions vs. experimental data for the particle-size distribution at Run 1.

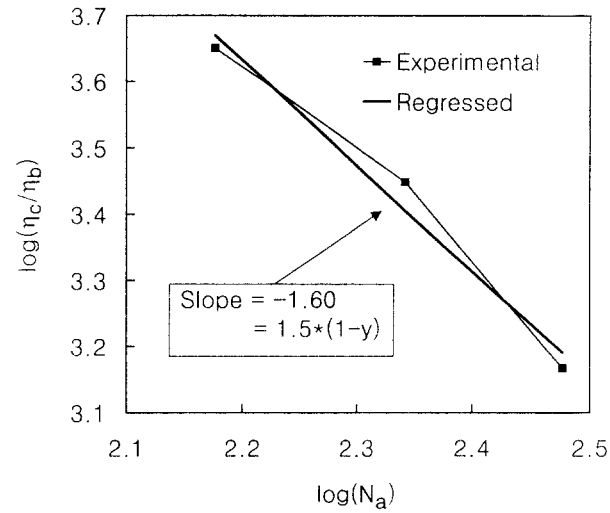

Figure 9. Estimation of the parameter y using the estimates of η_c/η_b obtained at different agitation speeds.

setting the operation variables so as to increase the η_c/η_b ratio. This is also confirmed in Table 2, which shows large estimates of η_c/η_b for the experiments whose distributions are biased toward coarse particles.

The first three runs in Table 2 for testing the effect of agitation speed deserve special attention in that the estimates of η_c/η_b provide a basis for inferring the parameter y. It is evident from Eq. 17 that η_c/η_b is proportional to G^{1-y} when the other variables are assumed to be constant. Using the relationship between G and P given in Eq. 3 and recalling that P is proportional to the cubic of the rpm N_a (McCabe et al., 1993), the following correlation can be deduced

$$\frac{\eta_c}{\eta_b} = CN_a^{1.5(1-y)}, \tag{24}$$

where C denotes a proportionality constant. The preceding correlation showed a fairly good linearity on a log-log plot, as illustrated in Figure 9. From the regressed value of the slope, y was estimated to be 2.07. This means that the breakup rate increases roughly in proportion to the square of the fluid shear rate, while the coagulation rate only rises linearly. Hence it can be concluded that intense agitation provides relatively more favorable conditions for breakup than for coagulation.

Conclusions

A modeling study has been carried out for ABS latex coagulation processes to investigate the effect of operation variables on the particle-size distribution of recovered resin powders. First, a kinetic model was presented for simultaneous coagulation and breakup of flocs in a turbulent flow field, and was converted into a discrete form using the general sectional balance. Then the population balance models were derived for batch and continuous processes, and were converted into dimensionless forms. Next, numerical algorithms for solving the models were constructed using an LSODE routine, and extensive simulations were performed to demon-

strate the model predictions. Finally, a set of batch experiments was carried out to verify the model predictions.

Our models contain two dimensionless groups, η_c and η_b, that pertain to the dynamics of coagulation and breakup, respectively. The η_c/η_b ratio represents the relative intensity of coagulation and breakup in the system, and thus acts as a design variable for controlling the steady-state particle-size distribution. The dimensionless groups comprise several operation variables and model parameters. Due to the lack of dynamic experimental data, the model parameters could not be uniquely determined except for y, which was inferred from the estimates of η_c/η_b for a set of batch experiments that differed only in the agitation speed. Nevertheless, the trend on how each operation variable affects the steady-state distribution can be comprehended through its contribution to the magnitude of the η_c/η_b ratio: a change of variable increasing the ratio will shift the size distribution toward larger particles. Specifically, increasing the slurry content of the latex and the coagulant dosage provides more favorable conditions to coagulation than breakup, while intense agitation favors breakup. The residence times of the continuous processes seem to have little effect under the current operating conditions where the kinetic terms dominate the process dynamics.

The present model has not taken into account the effect of temperature, which is regarded as an important factor for the aging of coagulated flocs. The model employs a simplified breakup kinetics that neglects erosion, breakup into more than two particles, and nonlinear breakup. Besides, the assumptions of constant collision efficiency and perfect mixing in the agitated tanks seem to represent other sources of structural modeling errors. A further investigation is needed to comprehend the consequences of these modeling errors on the particle-size distribution.

Acknowledgment

The first author (C.B.C.) acknowledges the partial financial support from KOSEF (Korea) through the Automation Research Center at POSTECH.

Literature Cited

Boadway, J. D., "Dynamics of Growth and Breakage of Alum Floc in Presence of Fluid Shear," *J. Environ. Eng. Div.: Proc. ASCE*, **104**, 901 (1978).

Camp, T. R., and P. G. Stein, "Velocity Gradients and Internal Work in Fluid Motion," *J. Boston Soc. Civ. Eng.*, **30**, 219 (1943).

Chen, W., R. R. Fisher, and J. C. Berg, "Simulation of Particle Size Distribution in an Aggregation-Breakup Process," *Chem. Eng. Sci.*, **45**, 3003 (1990).

Gelbard, F., Y. Tambour, and J. H. Seinfeld, "Sectional Representations for Simulating Aerosol Dynamics," *J. Colloid Interf. Sci.*, **76**, 541 (1980).

Gillespie, D. T., "The Stochastic Coalescence Model for Cloud Droplet Growth," *J. Atmos. Sci.*, **29**, 1496 (1972).

Hindmarsh, A. C., "Lsode and Lsodi, Two New Initial Value Ordinary Differential Equation Solvers," *ACM-Signum Newsletter*, **15**, 10 (1980).

Ives, K. J., "Coagulation and Flocculation: Part II. Orthokinetic Flocculation," *Solid-Liquid Separation*, 2nd ed., L. Svarovsky, ed., Butterworths, Boston, p. 86 (1981).

Lu, C. F., and L. A. Spielman, "Kinetics of Floc Breakage in Agitated Liquid Suspensions," *J. Colloid Interf. Sci.*, **103**, 95 (1985).

McCabe, W. L., J. C. Smith, and P. Harriott, *Unit Operations of Chemical Engineering*, 5th ed., McGraw-Hill, New York (1993).

Oles, V., "Shear-Induced Aggregation and Breakup of Polystyrene Latex Particles," *J. Colloid Interf. Sci.*, **154**, 351 (1992).

Pandya, J. D., and L. A. Spielman, "Floc Breakage in Agitated Suspensions: Theory and Data Processing Strategy," *J. Colloid Interf. Sci.*, **90**, 517 (1982).

Press, W. H., B. P. Flannery, S. A. Teukolsky, and W. T. Vetterling, *Numerical Recipes*, Cambridge Univ. Press, Cambridge (1986).

Quigley, J. E., and L. A. Spielman, "Strength Properties of Liquid Borne Flocs," Motion Picture, Project No. A-036-DEL, Water Resources Center, Univ. of Delaware, Newark (1977).

Saffman, P., and J. Turner, "On the Collision of Drops in Turbulent Clouds," *J. Fluid Mech.*, **1**, 16 (1956).

Spicer, P. T., and S. E. Pratsinis, "Coagulation and Fragmentation: Universal Steady-State Particle-Size Distribution," *AIChE J.*, **42**, 1612 (1996).

Spicer, P. T., S. E. Pratsinis, and M. D. Trennepohl, "Coagulation and Fragmentation: The Variation of Shear Rate and the Time Lag for Attainment of Steady State," *Ind. Eng. Chem. Res.*, **35**, 3074 (1996).

Valioulis, I. A., "Coagulation in the Aquatic Environment: Theory and Practice," *Adv. Colloid Interf. Sci.*, **24**, 81 (1986).

Manuscript received Dec. 8, 1997, and revision received Feb. 27, 1998.